IVYSPRING INTERNATIONAL PUBLISHER

Theranostics

2017; 7(15): 3803-3813. doi: 10.7150/thno.21068

Research Paper

A H_2O_2-Responsive Theranostic Probe for Endothelial Injury Imaging and Protection

Cheng-Kun Wang[1]*, Juan Cheng[1]*, Xing-Guang Liang[1], Chao Tan[1], Quan Jiang[1], Yong-Zhou Hu[1], Ying-Mei Lu[2], Kohji Fukunaga[3], Feng Han[1]✉ and Xin Li[1]✉

1. College of Pharmaceutical Sciences, Zhejiang University, 866 Yuhangtang Rd., Hangzhou 310058, China;
2. School of Medicine, Zhejiang University City College, 51 Huzhou Rd., Hangzhou 310015, China;
3. Department of Pharmacology, Graduate School of Pharmaceutical Sciences, Tohoku University, Aoba-Ku, Sendai 980-8578, Japan.

* These authors contributed equally to this work.

✉ Corresponding authors: F. Han. Tel: 86 571 88208402, Email: changhuahan@zju.edu.cn; X. Li. Tel: 86 571 88981051, Email: lixin81@zju.edu.cn

Received: 2017.05.17; Accepted: 2017.07.15; Published: 2017.08.23

Abstract

Overproduction of H_2O_2 causes oxidative stress and is the hallmark of vascular diseases. Tracking native H_2O_2 in the endothelium is therefore indispensable to gain fundamental insights into this pathogenesis. Previous fluorescent probes for H_2O_2 imaging were generally arylboronates which were decomposed to emissive arylphenols in response to H_2O_2. Except the issue of specificity challenged by peroxynitrite, boric acid by-produced in this process is actually a waste with unknown biological effects. Therefore, improvements could be envisioned if a therapeutic agent is by-produced instead. Herein, we came up with a "click-to-release-two" strategy and demonstrate that dual functional probes could be devised by linking a fluorophore with a therapeutic agent *via* a H_2O_2-responsive bond. As a proof of concept, probe **AP** consisting of a 2-(2'-hydroxyphenyl) benzothiazole fluorophore and an aspirin moiety has been prepared and confirmed for its theranostic effects. This probe features high specificity towards H_2O_2 than other reactive species including peroxynitrite. Its capability to image and ameliorate endothelial injury has been verified both *in vitro* and *in vivo*. Noteworthy, as a result of its endothelial-protective effect, **AP** also works well to reduce thrombosis formation in zebrafish model.

Key words: theranostic probe, fluorescent imaging, hydrogen peroxide, endothelial injury, oxidative stress.

Introduction

Endothelial dysfunction is critically involved in the pathogenesis of cardio- and cerebro-vascular diseases [1]. Although the underlying molecular mechanisms responsible for this pathological cascade remain elusive, it is affirmative that oxidative stress contributes to the etiology [2]. Reactive oxygen species (ROS) are therefore considered as crucial detrimental factors in the initiation and progression of neurovascular and cardiovascular disorders [3, 4]. As a prime member of the ROS family, hydrogen peroxide (H_2O_2) has been implicated in severe pathological conditions such as stroke [3, 4]. Aberrant levels of H_2O_2 in endothelial cells can imbalance redox state, destroy endothelial function and result in cellular damage [5, 6]. As a pro-oxidant molecule, H_2O_2 is mainly converted from superoxide spontaneously or following dismutation by superoxide dismutase [7]. It is subsequently scavenged by enzymes such as glutathione peroxidase (GPx), catalase, thioredoxins, or peroxiredoxins (Prx) [8-10]. H_2O_2 may also be converted to highly reactive hydroxyl radical either by exposure to ultraviolet light or *via* Fenton or Haber-Weiss reactions [11, 12]. H_2O_2 can oxidize macromolecules such as lipids, proteins and DNA to cause cytotoxic damage [13-15]. Nevertheless, on the contrary to its evil "Mr. Hyde" side, recent findings have lighted up its "Dr. Jekyll" role as a second

messenger with pro-survival function in several physiological processes [16-18]. As a Janus molecule, H_2O_2 has inspired great research interest on its role during redox signaling. It has been presumed that whether H_2O_2 is evil or good is determined largely by the context of production, local concentration, trafficking and consumption [19], which highlights the importance of detecting H_2O_2 dynamically in live organisms.

Numerous strategies have been developed to detect H_2O_2, including redox-sensitive fluorescent proteins [20-22], nanotubes [23, 24], hyperpolarization [25], ultrasound [26], mass spectrometry [27], PET [28], chemiluminescence [29,30], and H_2O_2-responsive small-molecule fluorescent probes [31-34], with the last one attracting particular interest due to its nondestructive nature and high sensitivity. To address the issue of lacking ROS specificity of commercially available probes such as dichlorodihydrofluorescein and dihydrorhodamine [35], Chang laboratory have pioneered with aryl boronate-based probes that are capable of undergoing biocompatible reactions with H_2O_2 to produce phenols [36-41]. This innovation has benefited research on H_2O_2 biology and led to fruitful results [42]. Importantly though, however, these aryl boronate-based probes are potentially threatened by their off-target reaction with peroxynitrite ($ONOO^-$) which is far more reactive than H_2O_2, albeit exists of much lower abundance [43]. Furthermore, boric acid by-produced in this process exists as a waste with unknown bioeffect (Figure 1). It is therefore envisioned that improvements could be made to devise new probes which release, instead of boric acid, but an agent helpful to ameliorate vascular damage accompanying the fluorescent signal. In our continuous research on the roles of redox-chemistry in the progression of vascular diseases [44], we report herein a theranostic probe that can not only sense H_2O_2 with high specificity, but is capable of neutralizing the oxidative damage incurred.

Experimental section

Materials

Dry dichloromethane (DCM) was distilled from CaH_2. Other reagents and chemicals for probe synthesis were obtained from commercial suppliers and used without further purification. Reactions were run under a nitrogen atmosphere and monitored by thin-layer chromatography (TLC) carried out on Silica gel 60 F254 plates supplied by Qingdao Puke Separation Material Corporation, and UV light was used as the visualizing agent. Flash column chromatography was performed using 200-300 mesh silica gel supplied by Qingdao Marine Chemical Factory, Qingdao, China.

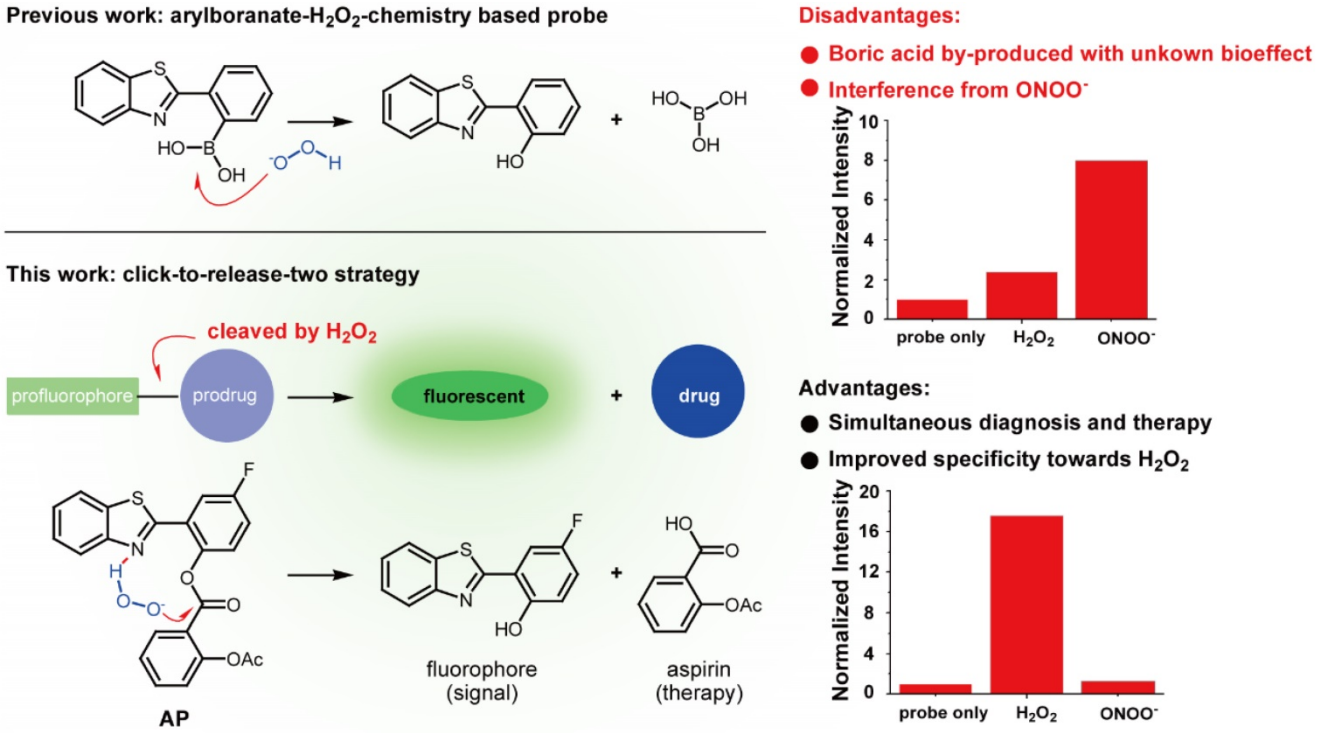

Figure 1. Comparison of previous arylboranate-H_2O_2 chemistry-based probe, and probe **AP** in this work. For the same fluorophore, boric acid-based probe showed poor selectivity for H_2O_2, while aspirin-based probe **AP** was almost immune to $ONOO^-$. Data were the normalized fluorescent intensity of the probes (10 μM) at 460 nm before or after the treatment of H_2O_2 (500 μM) or $ONOO^-$ (20 μM) for 30 min.

Reagents for biological experiments: Dulbecco's Modified Eagle's Medium (DMEM) was purchased from Invitrogen, and fetal bovine serum (FBS) from Gibco (Carlsbad, CA). Unless otherwise stated, all other reagents and chemicals were obtained from Sigma–Aldrich (St. Louis, MO). Hydrogen Peroxde Assay Kit was from Beyotime Biotechnology.

Instruments

^{1}H NMR spectra were obtained on a Bruker Fourier transform spectrometer (500 MHz) at 25 °C. ^{13}C NMR spectra were recorded on a Bruker Fourier transform spectrometer (125 MHz) spectrometer. All NMR spectra were calibrated using the residual solvent ($CDCl_3$) as internal reference (^{1}H NMR = 7.26, ^{13}C NMR = 77.16). All chemical shifts were reported in parts per million (ppm) and coupling constants (J) in Hz. The following abbreviations were used to explain the multiplicities: d = doublet, t = triplet, m = multiplet. IR spectra were taken on a Bruker Vector 22 spectrophotometer as KBr pellets. High resolution mass spectra (HRMS) were measured on an Agilent 6224 TOF LC/MS spectrometer using ESI-TOF (electrospray ionization-time of flight). The reaction process between **AP** and H_2O_2 was monitored on a SHIMADZU LCMS-2020 spectrometer. UV-Vis spectra were taken on a HITACHI U-3010 Spectrophotometer. Fluorescence measurements were conducted on an Agilent Cary Eclipse Fluorescence Spectrophotometer with slit widths to be 10 and 10 nm for excitation and emission respectively, and the photomultiplier (PMT) detector voltage was set at medium.

Probe synthesis and characterization

Procedures for the synthesis of probe **AP1-AP4** were detailed in the supplementary information. For the synthesis of probe **AP**, aspirin (0.10 g, 0.56 mmol) was dissolved in dry dichloromethylene (25 mL) and the mixture was cooled to 0 °C with an ice bath. Dry DMF (0.10 mL, 1.3 mmol) and oxalyl chloride (95 μL, 1.1 mmol) were then subsequently added to the mixture dropwise under a nitrogen atmosphere. The reaction was stirred at ambient temperature for 8 h, after which the volatile parts were removed by rotary evaporation. The residue was dissolved in dry dichloromethylene (20 mL), cooled to 0 °C, and then treated subsequently with 2-(2'-hydroxy-4'-fluorophenyl) benzothiazole (0.10 g, 0.41 mmol) and Et_3N (76 μL, 0.56 mmol). The mixture was stirred at ambient temperature for 8 h, after which H_2O (2.0 mL) was added to quench the reaction. The mixture was diluted with dichloromethylene (30 mL) and then transferred to a separatory funnel. The organic phase was washed with H_2O (2 × 20 mL) and brine (1 × 20 mL), dried over anhydrous Na_2SO_4, and concentrated under reduced pressure to give the crude product which was purified by flash column chromatography (SiO_2, petroleum ether/EtOAc, 20:1) to yield probe **AP** as a white solid (35 mg, 21% yield).

R_f = 0.55 (20:1, petroleum ether:EtOAc). **^{1}H NMR (500 MHz, $CDCl_3$, δ):** 8.43 (dd, *J* = 7.9, 1.6 Hz, 1H), 8.15 (dd, *J* = 9.2, 2.9 Hz, 1H), 7.99 (d, *J* = 8.1 Hz, 1H), 7.85 (d, *J* = 8.0 Hz, 1H), 7.73 (td, *J* = 8.0, 1.6 Hz, 1H), 7.48 (tt, *J* = 7.5, 1.0 Hz, 2H), 7.38 (t, *J* = 7.5 Hz, 1H), 7.31 – 7.23 (m, 3H), 2.27 (s, 3H). **^{13}C NMR (126 MHz, $CDCl_3$, δ):** 169.74 (d, *J* = 10.2 Hz), 162.72, 160.97, 160.54 (d, *J* = 246.6 Hz), 152.84 (d, *J* = 5.7 Hz), 151.76, 144.23 (d, *J* = 3.5 Hz), 135.67, 135.15 (d, *J* = 9.0 Hz), 132.84 (d, *J* = 3.3 Hz), 128.13, 126.60 (d, *J* = 3.3 Hz), 126.42 (d, *J* = 6.5 Hz), 125.75 (d, *J* = 2.6 Hz), 125.56, 124.35 (d, *J* = 1.9 Hz), 123.69, 122.36 (d, *J* = 8.0 Hz), 121.65 (d, *J* = 3.3 Hz), 118.53 (d, *J* = 23.8 Hz), 116.68 (d, *J* = 25.7 Hz), 21.10 (d, *J* = 5.5 Hz). **IR (KBr, cm^{-1}):** 3467, 3072, 2361, 1753, 1499, 1423, 1243, 1190, 1040, 754. **ESI-HRMS (*m/z*):** $[M+H]^+$ calc'd. for $C_{22}H_{15}FNO_4S$: 408.0706; found 408.0708.

Fluorometric analysis

Deionized water was used to prepare all aqueous solutions. All the photophysical characterization experiments were carried out at 37 °C. Phosphate buffer saline (PBS, 100 mM, pH 7.4) was purged with nitrogen for 5 min before use. **AP** was dissolved in DMSO to make a 10 mM stock solution. H_2O_2 and other reactive bio-relevant species were prepared as previously described [44]. To test the fluorescent responses of **AP** towards H_2O_2 or other reactive species, aliquots of probe stock solution were diluted with PBS (with 1‰ cetrimonium bromide) and treated with analytes to make sure both probes and analytes were kept at desired final concentrations. After quick and vigorous shaking, the mixture was allowed standing in the dark at 37 °C for desired time and the fluorescent spectra were then recorded under excitation at 375 nm. The emission spectra were scanned from 400 to 600 nm. All fluorometric experiments were performed in triplicate, and data shown were the average.

Cell culture

EA.hy926 cell line was purchased from ATCC (ATCC CRL-2922). EA.hy926 cells were grown in DMEM medium supplemented with 10% fresh bovine serum in a humidified atmosphere containing 5% CO_2 at 37 °C. Cultured cells without treatment served as controls.

Confocal fluorescence imaging methods

Cells were cultured on glass cover slips overnight and then pre-treated with **AP** for 15 min,

followed by being exposed to H_2O_2 for indicated time. Cells were then fixed in 4% polyformaldehyde. Nuclei were stained with propidium iodide (PI, sigma) in PBS after fixation. Probe fluorescence in EA.hy926 cells were visualized by confocal microscopy (Nikon A1R) and data were analysed using Image J software (NIH, Bethesda, MD, USA).

CCK-8 assay for cytotoxicity

A Cell Counting Kit-8 (CCK-8) assay (Dojindo; CK04) was used to measure cell viability. EA.hy926 cells were seeded in a 96-well plate at a density of 2.5 × 10^3 cells per well and incubated overnight. Cells were treated with different concentrations of probe **AP** or negative control for 24 h, then the medium was changed to fresh one (100 μl) and CCK-8 reagent (10 μl) was added. Following 1 h of incubation, cell viability was determined by measuring the optical absorbance at 450 nm with a multimode reader (Beckman Coulter; DTX880).

Oxygen and glucose deprivation (OGD) exposure

The oxygen and glucose deprivation (OGD) model was used to mimic the ischemia-like condition in live cells [45]. Briefly, cell culture medium was replaced with glucose-free HBSS (Hank's balanced salt solution), and cells were then placed in an airtight experimental hypoxia chamber (Billups-Rothenberg) containing a gas mixture of 95% N_2 and 5% CO_2. Cells were exposed to OGD for 0.5, 1 and 2 h to induce injury. Cells without OGD treatment were served as controls.

Middle cerebral artery occlusion (MCAO) model

The transient ischemia/reperfusion MCAO model was used to stimulate overproduction of H_2O_2 in mice. Model preparation was carried out as previously described [45]. Animal procedures were approved by the Committee on Animal Experiments at the Zhejiang University. The mice were subjected to one hour of ischemia followed by reperfusion. The brain was then isolated and slices were prepared 24 h after ischemia. The slices were then treated with probe **AP** for 15 min, and visualized by confocal microscopy (Nikon A1R). Data were analysed using Image J software (NIH, Bethesda, MD, USA).

Zebrafish care and maintenance

A wild-type AB strain of zebrafish (Batch Number 20150319) was used in the present study. The zebrafish were housed in a light and temperature controlled aquaculture facility with a standard 14-10 h light-dark conditions and fed with live brine shrimp twice daily and dry flake once a day. Four to five pairs of zebrafish were set up for natural mating every time, 200–300 embryos can thereby be generated. Embryos were maintained at 28 °C in fish water (0.2% Instant Ocean Salt in deionized water, pH 6.9–7.2, conductivity 480–510 μs/cm, and hardness 53.7–71.6 mg/L $CaCO_3$). Embryos were washed and staged at 6 and 24 hpf (hours post fertilization).

Zebrafish thrombosis model

3-Dpf zebrafish were chosen to prepare thrombosis model using a platelet agonist (arachidonic acid, 80 μM) challenge method. Zebrafish treated with 0.1% DMSO was served as a vehicle control. Zebrafish from each group were randomly selected for visually qualitative assessment of the thrombus formation in the caudal vein at the lateral view with a dissecting stereomicroscope. The resting zebrafish were stained with *O*-dianisidine to quantify the heart red blood cells (RBCs) (hemoglobin level) which reversely correlated with the degree of thrombosis. The optimal concentration and incubation time of arachidonic acid treatment were selected according to the qualitative and quantitative results of thrombosis. Heart RBCs counts were performed using the NIS-Elements D3.10 image analysis software (Nikon). The effect of a test drug was calculated based on the formula below:

$$\text{Efficacy (\%)} = [[S(\text{drug})-S(\text{model})]/[S(\text{vehicle})-S(\text{model})]]\text{x}100\%$$

A positive percentage means that a tested drug could prevent and/or treat thrombus and a negative percentage suggests that the tested drug had no effect on thrombosis in the zebrafish model.

Results and Discussion

Initially, to fulfill the task of therapy, aspirin was judiciously selected as the prime building block attributing to its vascular-beneficial effects such as antioxidant, anti-inflammatory and antiplatelet [46]. In particular, aspirin is not only efficient in reducing stroke incidence, but can also attenuate clinical deficits at stroke onset [47]. To orchestrate the therapeutic effect of aspirin with a fluorescent diagnostic signal for H_2O_2, it should be combined with a fluorophore *via* a H_2O_2-sensitive linkage. Since H_2O_2 with p*K*a of 11.75 is slightly more acidic than H_2O (p*K*a 13.99), we surmised that H_2O_2 in neutral aqueous solution might catalyze the hydrolysis of certain esters. Therefore, aspirin was combined with 2-(2'-hydroxy-4'-fluorophenyl) benzothiazole fluorophore with an ester bond to construct probe **AP** (Figure 1). We reasoned that the ester bond would block the excited state intramolecular proton transfer process (ESIPT) in the fluorophore which is essential

for illumination [48], whereas the nitrogen atom on the fluorophore skeleton could bring HOO^- within close proximity to the ester *via* a hydrogen bonding to accelerate the hydrolysis. **AP** was facilely prepared as detailed in the experimental section.

The optical response of **AP** towards H_2O_2 was tested in PBS (100 mM, pH 7.4). As shown in Figure 2A, **AP** showed the absorption maximized at 297 nm (*c* 30 μM, 15 463 M^{-1} cm^{-1}). Treatment of H_2O_2 (1.0 mM) induced a time-dependent decrease of the original peak and the emergence of a new red-shifted band peaked at 336 nm, indicating the slow hydrolysis of the ester to yield the -OH group as a better auxochrome. Coinciding with the UV-Vis absorption response, H_2O_2 treatment also induced a time-dependent increase of **AP** fluorescence centred at 476 nm (Figure 2B, Figure S1-S4). When the response was observed over longer time, completion could be detected in 2 hours (Figure S5). Furthermore, **AP** (10 μM) responded to H_2O_2 with fluorescence enhancement in a dose-dependent manner (Figure 2C) with H_2O_2 concentrations higher than 1 mM bringing the response to its maximum (F_{max}). Interestingly, the Napierian logarithm of F_{max} minus F correlated linearly with H_2O_2 concentrations in the range of 0-500 μM (Figure S6, S7). Notably, the detection limit of the probe was found to be as low as 2.5 μM (Figure S8). These results suggest the great potential of probe **AP** to quantify H_2O_2 in PBS medium. The selectivity of **AP** towards various reactive species was also evaluated. Among the various biologically-relevant reactive species, only H_2O_2 was found capable of triggering on the fluorogenic response of **AP** with a 11-fold intensity increase, which is at least 8-fold more selective than $ONOO^-$, a common interferent for boronate-based probes (Figure 2D and Figure S9). Furthermore, the effect of pH on the stability of probe **AP** was also studied. **AP** is quite stable below pH 7.0. Though slight hydrolysis of the ester group was observed at pH 7.5 as indicated by the 2.6 folds of fluorescence intensity increase, this increase is much smaller than

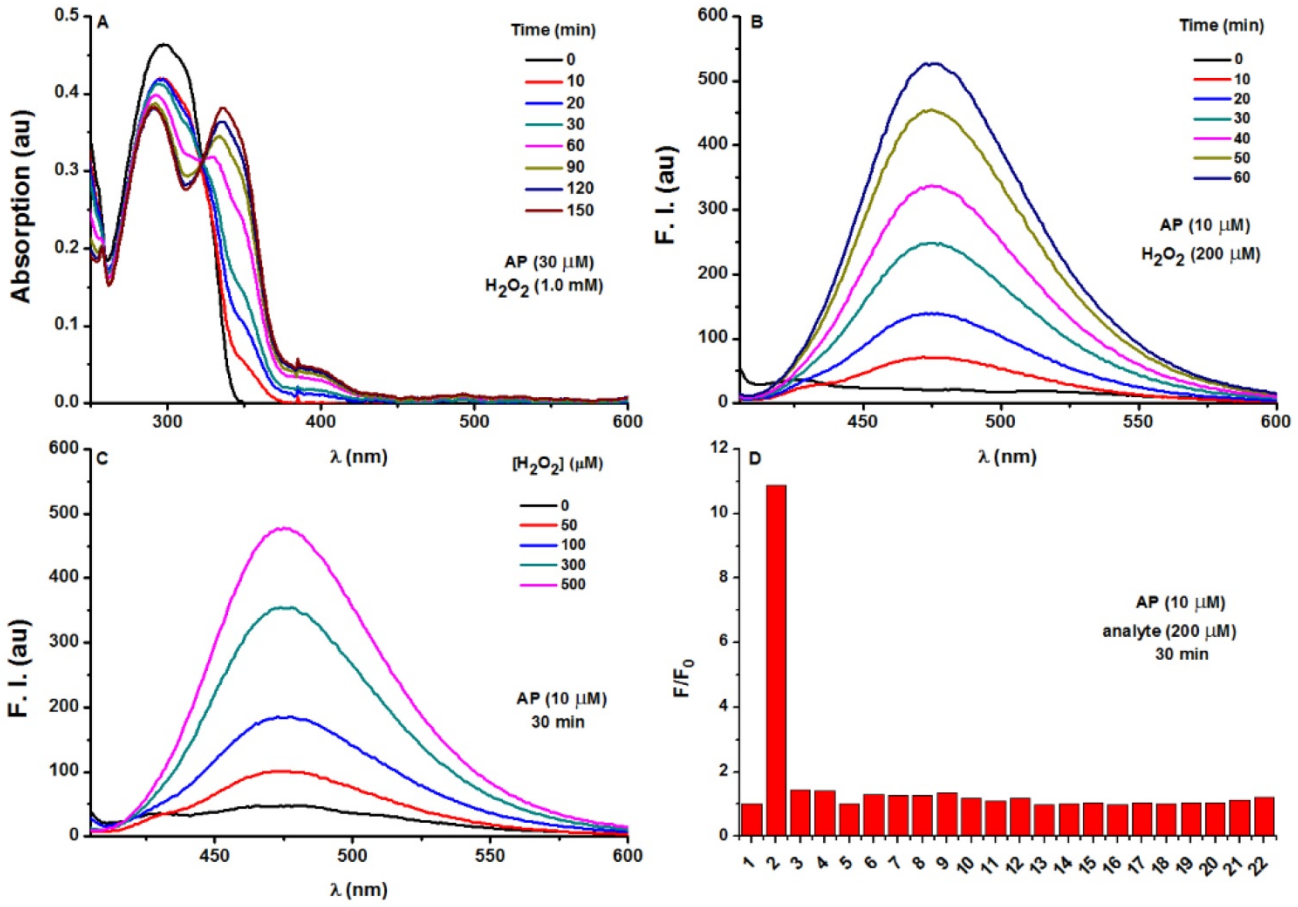

Figure 2. Photophysical responses of **AP** to H_2O_2. A) UV-Vis absorption response of **AP** (30 μM) towards H_2O_2 (1.0 mM) as time lapsed. B) Fluorescence response of **AP** (10 μM) towards H_2O_2 (200 μM) as time lapsed. C) Fluorescence response of **AP** (10 μM) towards various concentrations of H_2O_2 at a time point of 30 min. D) Fluorescent responses of **AP** (10 μM) toward various analytes (200 μM) after a reaction time of 30 min, where F represents the fluorescent intensity of **AP** at 476 nm after the treatment of various analytes, and F_0 represents the intensity of blank **AP** solution at 476 nm. (1) probe blank, (2) H_2O_2, (3) $^1O_2$, (4) O_2^-, (5) ClO^-, (6) THBP, (7) $ONOO^-$, (8) NO, (9) NO_2^-, (10) NO_3^-, (11) GSH, (12) Cys, (13) Hcy, (14) Gly, (15) Ala, (16) Mg^{2+}, (17) Ca^{2+}, (18) Fe^{3+}, (19) Fe^{2+}, (20) K^+, (21) Cu^{2+}, (22) Zn^{2+}. All fluorescence data were collected in PBS (pH 7.4, 100 mM) at 37°C with λ_{ex} 375 nm. UV data were obtained in PBS with 50% EtOH as co-solvent.

that caused by H_2O_2 (Figure S10). Given the fact that cytosol generally has a pH of 7.2 and most organelles are below pH 7.2 [49], probe **AP** should be stable enough to stand cellular pH gradients.

With the fluorogenic response of probe **AP** towards H_2O_2 systematically characterized, we next evaluated if aspirin would be released in this process as surmised in Figure 1. The reaction between **AP** and H_2O_2 in PBS was therefore tracked by LC-MS analysis to determine the structures of the products. Prior to this study, the LC-MS spectra of a mixture of **AP**, 2-(2'-hydroxy-4'-fluophenyl) benzothiazole fluorophore, aspirin and salicylic acid were recorded for reference. It turned out that treatment of **AP** with H_2O_2 induced a gradual decrease of the probe, accompanied by the simultaneous increase in the formation of the free fluorophore and aspirin in the form of salicylic acid (Figure S11-S15), indicating the efficient release of aspirin and the fluorophore triggered by H_2O_2. To make further confirmation, probe **AP** was treated with H_2O_2 in a flask, and 2-(2'-hydroxy-4'-fluophenyl) benzothiazole fluorophore was isolated and characterized by ^1H NMR, further consolidating the mechanism shown in Figure 1 (Figure S16).

To find out if other fluorophores could also work in this design, probe **AP1**-**AP4** were prepared by esterifying the phenol hydroxyl group in an acylnaphthalene, coumarin, naphthalimide, or hemicyanine (Figure S17). When their responses towards H_2O_2 were tested in comparison with probe **AP**, all the probes were found active with probe **AP** being the most sensitive one (Figure S18). This result demonstrates the generality of the acetosalicylic phenolic ester as a H_2O_2-responsive trigger.

Having confirmed H_2O_2-triggered release of the free fluorophore and aspirin from probe **AP** in aqueous solution, we moved on to investigate the feasibility of **AP** to image H_2O_2 in EA.hy926 endothelial cells by confocal fluorescence microscopy. For this purpose, the cytotoxicity of probe **AP** was first evaluated by CCK8 assay. After treating EA.hy926 cells with various concentrations of **AP**, cell viability was monitored with a CCK8 kit and no significant **AP** toxicity was observed (Figure S19). Then, the response of EA.hy926 cells to probe **AP** was recorded. As shown in Figure 3, almost no detectable fluorescence signal was observed in control cells loaded with only probe **AP**. However, significant elevation of **AP** fluorescence was observed when the cells were exposed to exogenous H_2O_2, and the intracellular fluorescence increased in a H_2O_2 dose-dependent way. Time-dependent increase of **AP** fluorescence was also observed after the cells were exposed to H_2O_2 (50 μM) (Figure S20). Noteworthy, similar results were obtained in HUVEC cells, for which exogenous H_2O_2 exposure resulted in both H_2O_2 dose-dependent and time-dependent intensification of intracellular fluorescence (Figure S21, S22), indicating the potential of **AP** to track H_2O_2 levels in live cells.

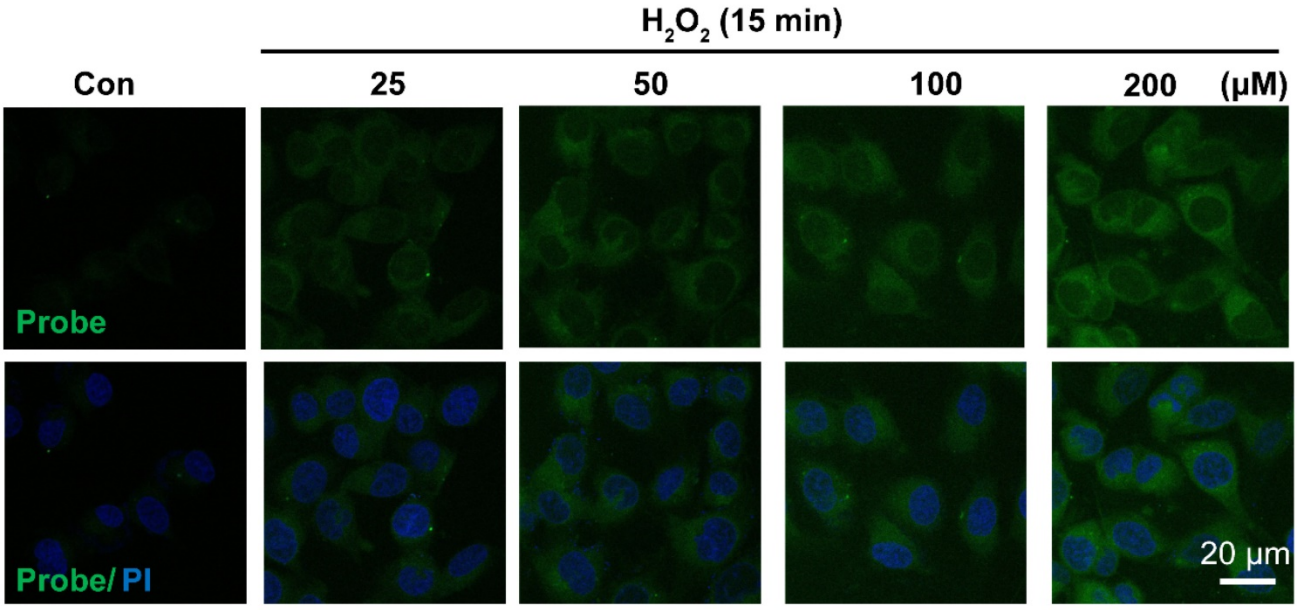

Figure 3. Representative confocal images showed dose-dependent increase of **AP** fluorescence in endothelial cells. Cells were seeded on 24-well glass cover slips overnight and then pre-incubated with **AP** (5.0 μM) for 15 min, followed by challenging without or with H_2O_2 (25-200 μM) for 15 min. **AP** fluorescence (green, 460 nm) was excited at 405 nm. PI counterstaining indicated nuclear localization (blue, 620 nm). All images were captured using a Nikon A1R confocal microscope with the same settings. Overlay image of all captured fluorescence intensities are shown. Scale bar represents 20 μm.

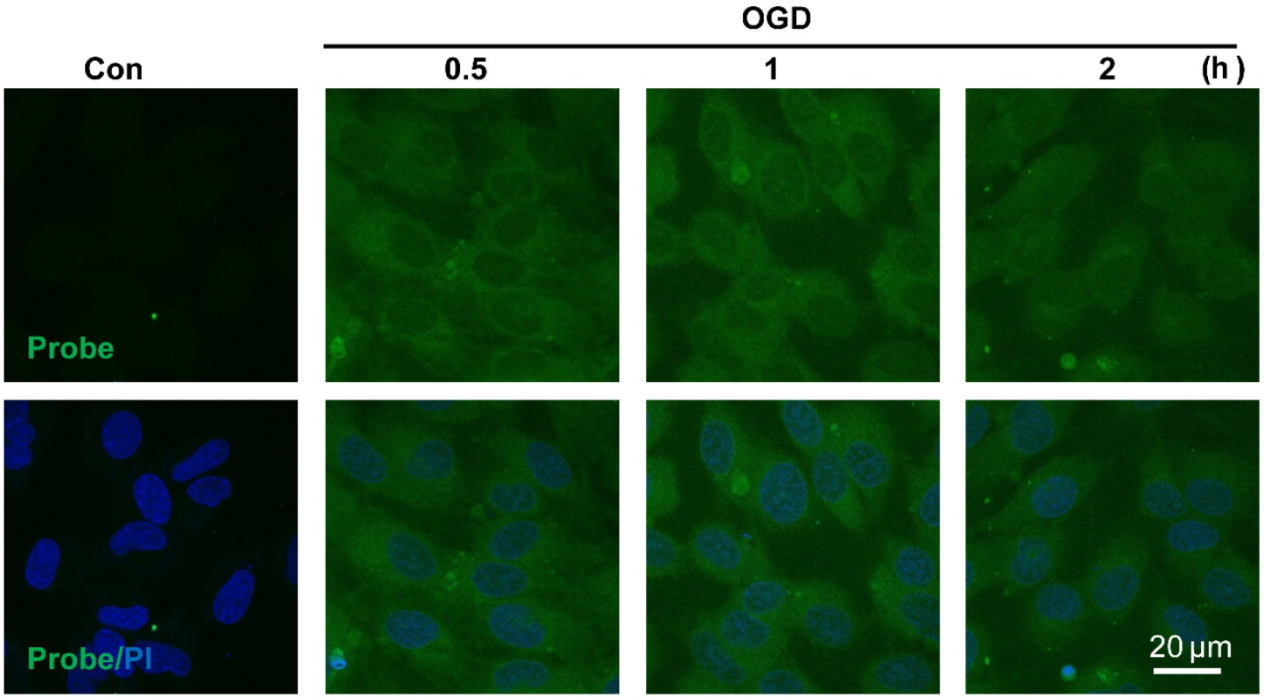

Figure 4. Visualizing endogenous H_2O_2 formation using **AP** in endothelial cells following oxygen-glucose deprivation (OGD). The representative confocal images showed temporal changes of **AP** fluorescence (green, 460 nm) in EA.hy926 endothelial cells over 0.5 to 2 h following OGD. PI counterstaining indicated nuclear localization (blue, 620 nm). Overlay image of **AP** fluorescence and PI are shown. Scale bar represents 20 μm.

The sensitivity of probe **AP** to image endogenous H_2O_2 in live cells was also tested. Since aberrant accumulation of H_2O_2 has been reported in the progression of ischemic endothelial injury [50], we therefore evaluated if probe **AP** could track the dynamic change of endogenous H_2O_2 formation during endothelia injury. For this purpose, oxygen-glucose deprivation (OGD) stimulation model was employed to induce ischemic endothelial injury, and the fluorescent response of live cells after OGD stimulation was recorded. We first confirmed that probe **AP** was inert to OGD reagents (Figure S23). When EA.hy926 cells subjected to OGD treatment over 0.5-2 h were stained with **AP**, time-dependent accumulation of intracellular **AP** fluorescence was observed, which agreed well with the staining results obtained with a commercial Hydrogen Peroxde Assay Kit (Beyotime Biotechnology) (Figure S24), indicating the sensitivity of **AP** for endogenous H_2O_2 in live cells. This result also reveals the quick destroy of native redox homeostasis and the emergence of a more oxidative environment within endothelial cells upon injury, which is in agreement with previous reports [50].

Having confirmed the ability of probe **AP** to image H_2O_2 accumulation during endothelial cell injury, we moved on to investigate if H_2O_2-triggered release of aspirin would display therapeutic effect against H_2O_2-induced endothelial apoptosis. Cell apoptosis was determined using flow cytometry with annexin V-FITC/propidium iodide (PI). We first confirmed that probe **AP** (25 μM) by itself had no adverse effect on cell viability as **AP** treatment gave similar staining results as the control group. Furthermore, H_2O_2 (200 μM, 2 h) treatment was found to significantly induce elevation in the fraction of annexin V/PI positive cells (14.90%) compared to the control group (1.90%), suggesting its cytotoxicity. By contrast, **AP** incubation significantly reduced H_2O_2-induced cell apoptosis (2.90%; Figure 5A and Figure S25). Interestingly, this was particularly evident in HUVEC by flow cytometry assay (Figure S26). Furthermore, the protective effect of probe **AP** against H_2O_2-induced endothelial cell apoptosis was confirmed by reduced phosphorylation of JNK, ERK and p38 in H_2O_2-**AP**-treated cells in compare to H_2O_2-treated ones (Figure 5B-5E). Taken together, these data support the bifunctional roles of **AP** either for live cell imaging or to ameliorate endothelial injury during H_2O_2-induced oxidative stress.

Having confirmed the good performance of probe **AP** in live cells, we next expand the scope to live tissues, and a middle cerebral artery occlusion (MCAO) model was used to induce oxidative damage to the brain neurovascular system. Mice brain was isolated 24 h after ischemia and slices were prepared. When the slices were stained with probe **AP**, strong **AP** fluorescence was observed in the brain ischemic

region of MCAO mice (Figure 6). However, no significant **AP** fluorescence was observed in the sham group. These results demonstrate the sensitivity and specificity of probe **AP** to image neurovascular cell injury.

To further confirm the endothelial-protective effect of probe **AP** in zebrafish model, its anti-thrombotic effect was evaluated with aspirin as a positive control, because endothelial cell injury has been considered as the underlying pathogenesis of microvascular thrombosis and ischemia. Zebrafish thrombosis model was prepared as described and hemoglobin staining was used to indicate the degree of intravascular thrombosis [51]. As shown in Figure 7, in contrast to the normal heart RBCs/hemoglobin staining in the control group, arachidonic acid (a platelet agonist) treatment resulted in only weak staining. However, probe **AP** (8.3 μM or 25 μM) treatment was observed to be able to significantly inhibit arachidonic acid-induced thrombosis formation in zebrafish compared to the vehicle group, and the potency was **AP** dose-dependent (Figure 7A-B). Furthermore, similar results were obtained in the caudal vein of Zebrafish with thrombosis (Figure 7C), for which the preventive efficacy on thrombosis formation was quantified to be 78% for aspirin (139 μM), 41% for probe **AP** (8.3 μM) and 52% for probe **AP** (25 μM), respectively (Figure 7D).

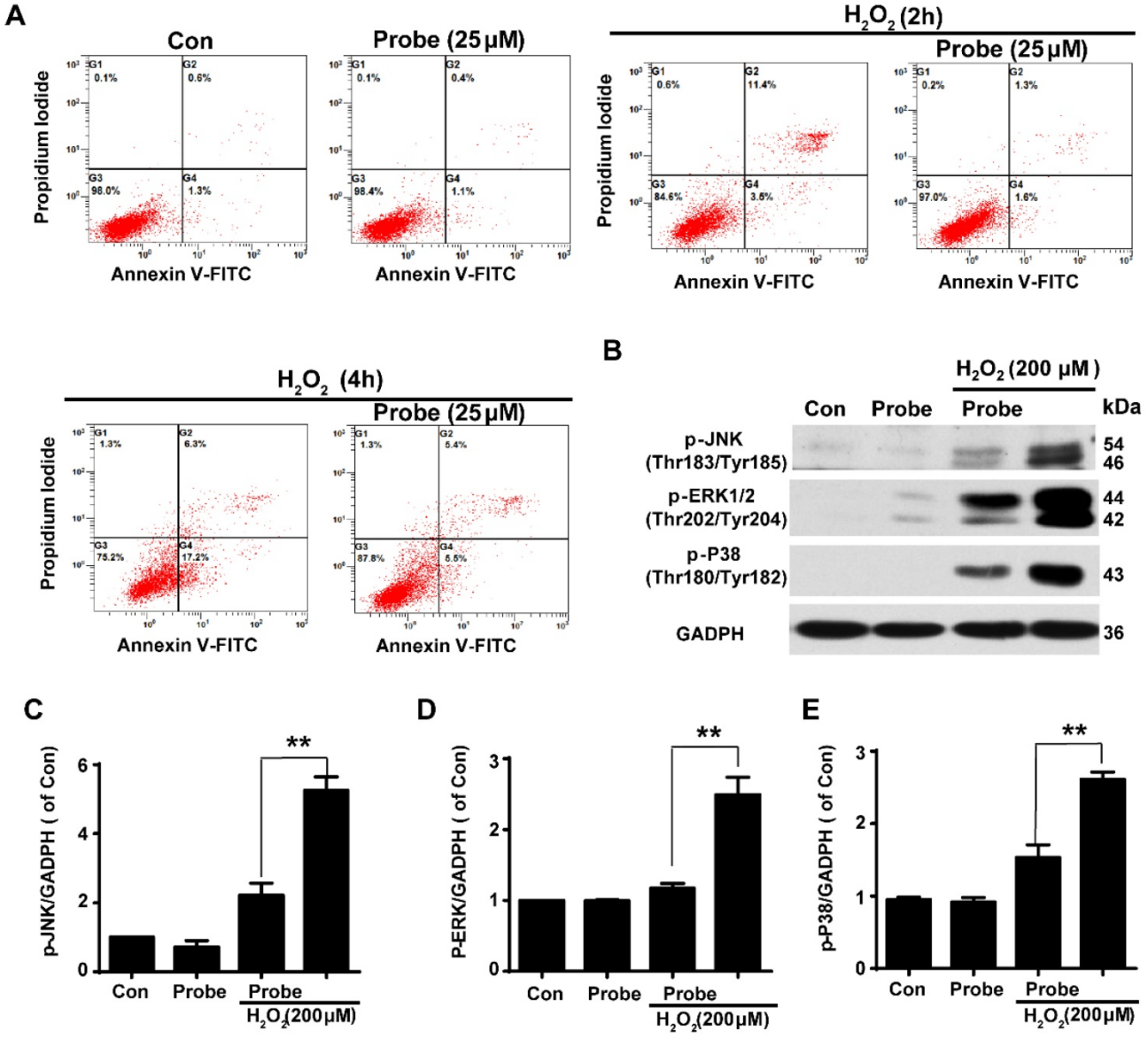

Figure 5. The protective role of **AP** against H_2O_2-induced endothelial apoptosis. A) The apoptosis of endothelial cells was labelled with annexin V-FITC/propidium iodide (PI) and determined using flow cytometry. EA.hy926 cells were seeded on 12-well plates overnight and then pre-incubated with **AP** (25 μM) for 15 min, followed by stimulation with H_2O_2 (200 μM, 2 h or 4 h) in HBSS medium. B) The representative blots for phosphorylation of JNK, ERK and p38 in the presence of **AP** probe upon H_2O_2 (200 μM, 12 h) exposure in DMEM medium. Summary of phospho-JNK (C), phospho-ERK (D) and phospho-p38 (E) were indicated as densitometric values. $^{**}p < 0.01$.

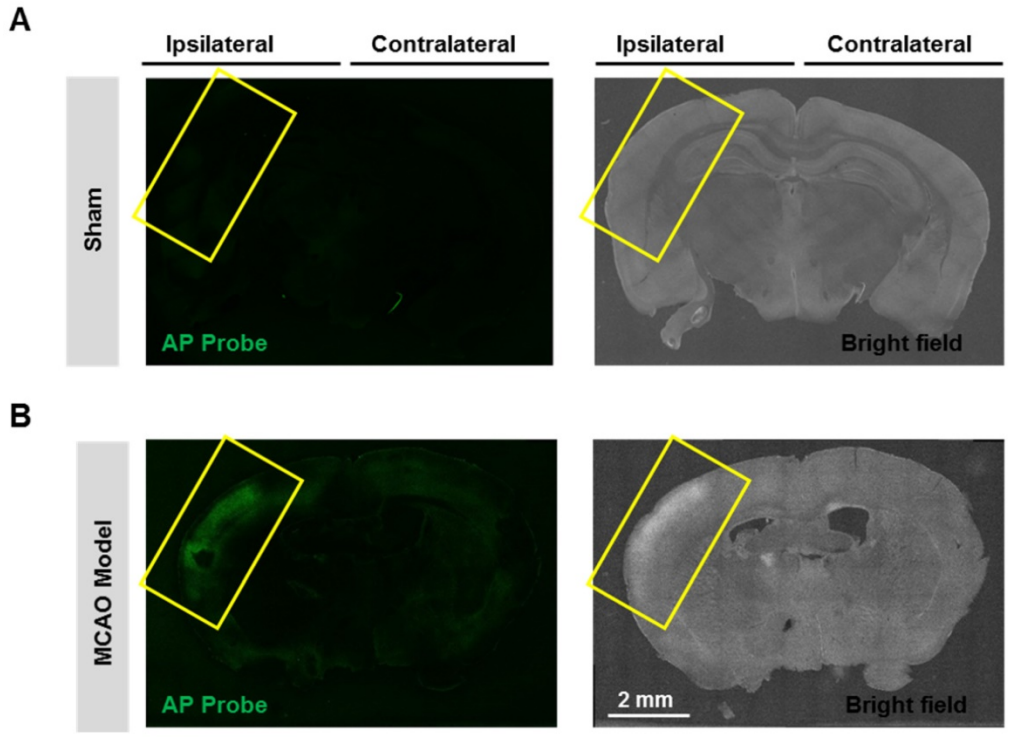

Figure 6. Visualizing endogenous H_2O_2 formation using **AP** in MCAO mouse. The representative confocal images showed changes of **AP** fluorescence (green) in brain ischemic region in MCAO mice. Insert frame: Brain ischemic region. Scale bar represents 2 mm.

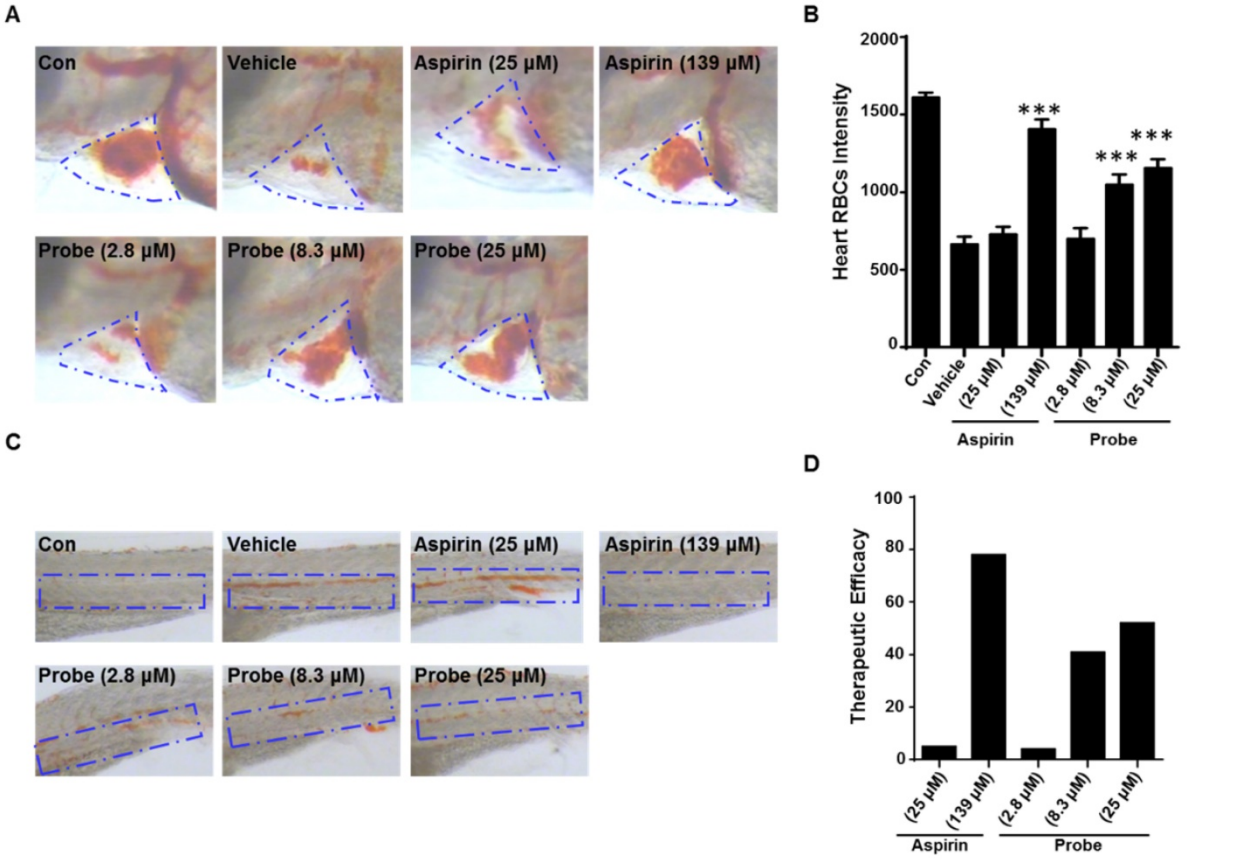

Figure 7. The antithrombotic effect of probe **AP**. Zebrafish treated with arachidonic acid for 1.5 h were used as thrombosis model. A) Effects of probe **AP** on heart RBCs in thrombotic zebrafish. The heart red blood cells were stained with *o*-dianisidine staining. The heart RBCs intensity of zebrafish increased following **AP** probe treatment (1.5 h) in the presence of arachidonic acid (80 μM). B) Quantification data for Figure A. C) Effect of **AP** probe on thrombus formation in the caudal vein under a dissecting stereomicroscope. Images from aspirin or **AP** probe treatment are shown from a representative caudal vein of zebrafish from each group. Thrombus formation was markedly reduced in zebrafish treated with **AP** probe (1.5 h) in the presence of arachidonic acid. D) The therapeutic efficacy of **AP** probe on thrombosis formation.

Conclusions

In summary, targeting the oxidative microenvironment of vascular diseases represented by the overproduction of H_2O_2, we have developed the first theranostic probe for its simultaneous imaging and neutralization by combining a fluorophore with an endothelial-protective agent *via* a H_2O_2-sensitive bond. The probe has been proven suitable for imaging native H_2O_2 generation in live cells, and is capable of eliciting protective effects against both H_2O_2-induced endothelial cell apoptosis and vascular pathology in Zebrafish thrombosis mode. The probe should hold promise to serve as a dual functional imaging tool to explore H_2O_2 signalling under a variety of pathological contexts. The design strategy illustrated in this work should be inspiring for future probe design.

Acknowledgement

This work was supported in part by National Key Research and Development Program of China (2016YFE0125400), National Natural Science Foundations of China (81473202, 81573411, 21642007), Zhejiang Provincial Natural Science Foundation of China (Z16H310003, LY15H300003), Zhejiang Provincial Science and Technology Planning Project (2017C33053), Zhejiang Province Program for Cultivation of High-level Health talents.

Supplementary Material

Figure S1-S26, synthesis and characterization of **AP1**-**AP4**, NMR traces of probe **AP**.
http://www.thno.org/v07p3803s1.pdf

Competing Interests

The authors have declared that no competing interest exists.

References

1. Vanhoutte PM, Shimokawa H, Tang EH, Feletou M. Endothelial dysfunction and vascular disease. Acta Physiol (Oxf). 2009; 196:193-222.
2. Kasote DM, Hegde MV, Katyare SS. Mitochondrial dysfunction in psychiatric and neurological diseases: cause(s), consequence(s), and implications of antioxidant therapy. Biofactors. 2013; 39:392-406.
3. McCann SK, Roulston CL. NADPH Oxidase as a Therapeutic Target for Neuroprotection against Ischaemic Stroke: Future Perspectives. Brain Sci. 2013; 3:561-98.
4. Schriewer JM, Peek CB, Bass J, Schumacker PT. ROS-mediated PARP activity undermines mitochondrial function after permeability transition pore opening during myocardial ischemia-reperfusion. J Am Heart Assoc. 2013; 2:e159.
5. Hao XL, Kang Y, Li JK, Li QS, Liu EL, Liu XX. Protective effects of hyperoside against H_2O_2-induced apoptosis in human umbilical vein endothelial cells. Mol Med Rep. 2016; 14:399-405.
6. Zhai L, Zhang P, Sun RY, Liu XY, Liu WG, Guo XL. Cytoprotective effects of CSTMP, a novel stilbene derivative, against H_2O_2-induced oxidative stress in human endothelial cells. Pharmacol Rep. 2011; 63:1469-80.
7. He C, Murthy S, McCormick ML, Spitz DR, Ryan AJ, Carter AB. Mitochondrial Cu, Zn-superoxide dismutase mediates pulmonary fibrosis by augmenting H_2O_2 generation. J Biol Chem. 2011; 286:15597-607.
8. Bagulho A, Vilas-Boas F, Pena A, et al. The extracellular matrix modulates H_2O_2 degradation and redox signaling in endothelial cells. Redox Biol. 2015; 6:454-60.
9. Rocha S, Gomes D, Lima M, Bronze-da-Rocha E, Santos-Silva A. Peroxiredoxin 2, glutathione peroxidase, and catalase in the cytosol and membrane of erythrocytes under H_2O_2-induced oxidative stress. Free Radic Res. 2015; 49:990-1003.
10. Miguel F, Augusto AC, Gurgueira SA. Effect of acute *vs* chronic H_2O_2-induced oxidative stress on antioxidant enzyme activities. Free Radic Res. 2009; 43:340-7.
11. Guntur AR, Gu P, Takle K, Chen J, Xiang Y, Yang CH. Drosophila TRPA1 isoforms detect UV light via photochemical production of H_2O_2. Proc Natl Acad Sci U S A. 2015; 112:E5753-61.
12. Yalfani MS, Contreras S, Medina F, Sueiras JE. Hydrogen substitutes for the *in situ* generation of H_2O_2: an application in the Fenton reaction. J Hazard Mater. 2011; 192:340-6.
13. Choi DJ, Kim SL, Choi JW, Park YI. Neuroprotective effects of corn silk maysin via inhibition of H_2O_2-induced apoptotic cell death in SK-N-MC cells. Life Sci. 2014; 109:57-64.
14. Kubota Y, Shimizu S, Yasuhira S, Horiuchi S. SNF2H interacts with XRCC1 and is involved in repair of H_2O_2-induced DNA damage. DNA Repair (Amst). 2016; 43:69-77.
15. Martins D, Titorenko VI, English AM. Cells with impaired mitochondrial H_2O_2 sensing generate less •OH radicals and live longer. Antioxid Redox Signal. 2014; 21:1490-503.
16. Stone JR, Yang S. Hydrogen peroxide: a signaling messenger. Antioxid Redox Signal. 2006; 8:243-70.
17. Sies H. Role of metabolic H_2O_2 generation: redox signaling and oxidative stress. J Biol Chem. 2014; 289:8735-41.
18. Rice ME. H_2O_2: a dynamic neuromodulator. Neuroscientist. 2011; 17:389-406.
19. Wang ZH, Liu JL, Wu L, Yu Z, Yang HT. Concentration-dependent wrestling between detrimental and protective effects of H_2O_2 during myocardial ischemia/reperfusion. Cell Death Dis. 2014; 5:e1297.
20. Schwarzländer M, Dick TP, Meyer AJ, Morgan B. Dissecting Redox Biology Using Fluorescent Protein Sensors. Antioxid Redox Signal. 2016; 24:680-712.
21. Bilan DS, Pase L, Joosen L, et al. HyPer-3: a genetically encoded H_2O_2 probe with improved performance for ratiometric and fluorescence lifetime imaging. ACS Chem Biol. 2013; 8:535-42.
22. Lukyanov KA, Belousov VV. Genetically encoded fluorescent redox sensors. Biochim Biophys Acta. 2014; 1840:745-56.
23. Sun Y, He K, Zhang Z, Zhou A, Duan H. Real-time electrochemical detection of hydrogen peroxide secretion in live cells by Pt nanoparticles decorated graphene-carbon nanotube hybrid paper electrode. Biosens Bioelectron. 2015; 68:358-64.
24. Mu B, Zhang J, McNicholas TP, Reuel NF, Kruss S, Strano MS. Recent advances in molecular recognition based on nanoengineered platforms. Acc Chem Res. 2014; 47:979-88.
25. Lippert AR, Keshari KR, Kurhanewicz J, Chang CJ. A hydrogen peroxide-responsive hyperpolarized ^{13}C MRI contrast agent. J Am Chem Soc. 2011; 133:3776-9.
26. Olson ES, Orozco J, Wu Z, et al. Toward in vivo detection of hydrogen peroxide with ultrasound molecular imaging. Biomaterials. 2013; 34:8918-24.
27. Cochemé HM, Quin C, McQuaker SJ, et al. Measurement of H_2O_2 within living Drosophila during aging using a ratiometric mass spectrometry probe targeted to the mitochondrial matrix. Cell Metab. 2011; 13:340-50.
28. Carroll V, Michel BW, Blecha J, et al. A boronate-caged [^{18}F]FLT probe for hydrogen peroxide detection using positron emission tomography. J Am Chem Soc. 2014; 136:14742-5.
29. Van de Bittner GC, Dubikovskaya EA, Bertozzi CR, Chang CJ. In vivo imaging of hydrogen peroxide production in a murine tumor model with a chemoselective bioluminescent reporter. Proc Natl Acad Sci U S A. 2010; 107:21316-21.
30. Van de Bittner GC, Bertozzi CR, Chang CJ. Strategy for dual-analyte luciferin imaging: in vivo bioluminescence detection of hydrogen peroxide and caspase activity in a murine model of acute inflammation. J Am Chem Soc. 2013; 135:1783-95.
31. Kolanowski JL, Kaur A, New EJ. Selective and Reversible Approaches Toward Imaging Redox Signaling Using Small-Molecule Probes. Antioxid Redox Signal. 2016; 24:713-30.
32. Lin VS, Dickinson BC, Chang CJ. Boronate-based fluorescent probes: imaging hydrogen peroxide in living systems. Methods Enzymol. 2013; 526:19-43.
33. Dickinson BC, Srikun D, Chang CJ. Mitochondrial-targeted fluorescent probes for reactive oxygen species. Curr Opin Chem Biol. 2010; 14:50-6.
34. Miller EW, Chang CJ. Fluorescent probes for nitric oxide and hydrogen peroxide in cell signaling. Curr Opin Chem Biol. 2007; 11:620-5.
35. Wardman P. Fluorescent and luminescent probes for measurement of oxidative and nitrosative species in cells and tissues: progress, pitfalls, and prospects. Free Radic Biol Med. 2007; 43:995-1022.
36. Miller EW, Albers AE, Pralle A, Isacoff EY, Chang CJ. Boronate-based fluorescent probes for imaging cellular hydrogen peroxide. J Am Chem Soc. 2005; 127:16652-9.
37. Srikun D, Miller EW, Domaille DW, Chang CJ. An ICT-based approach to ratiometric fluorescence imaging of hydrogen peroxide produced in living cells. J Am Chem Soc. 2008; 130:4596-7.
38. Dickinson BC, Chang CJ. A targetable fluorescent probe for imaging hydrogen peroxide in the mitochondria of living cells. J Am Chem Soc. 2008; 130:9638-9.

39. Srikun D, Albers AE, Nam CI, Iavarone AT, Chang CJ. Organelle-targetable fluorescent probes for imaging hydrogen peroxide in living cells via SNAP-Tag protein labeling. J Am Chem Soc. 2010; 132:4455-65.
40. Dickinson BC, Huynh C, Chang CJ. A palette of fluorescent probes with varying emission colors for imaging hydrogen peroxide signaling in living cells. J Am Chem Soc. 2010; 132:5906-15.
41. Lippert AR, Van de Bittner GC, Chang CJ. Boronate oxidation as a bioorthogonal reaction approach for studying the chemistry of hydrogen peroxide in living systems. Acc Chem Res. 2011; 44:793-804.
42. Fu X, Tang Y, Dickinson BC, Chang CJ, Chang Z. An oxidative fluctuation hypothesis of aging generated by imaging H_2O_2 levels in live Caenorhabditis elegans with altered lifespans. Biochem Biophys Res Commun. 2015; 458:896-900.
43. Brewer TF, Garcia FJ, Onak CS, Carroll KS, Chang CJ. Chemical approaches to discovery and study of sources and targets of hydrogen peroxide redox signaling through NADPH oxidase proteins. Annu Rev Biochem. 2015; 84:765-90.
44. Li X, Tao RR, Hong LJ, et al. Visualizing peroxynitrite fluxes in endothelial cells reveals the dynamic progression of brain vascular injury. J Am Chem Soc. 2015; 137:12296-303.
45. Tao RR, Wang H, Hong LJ, et al. Nitrosative stress induces peroxiredoxin 1 ubiquitination during ischemic insult via E6AP activation in endothelial cells both in vitro and in vivo. Antioxid Redox Signal. 2014; 21:1-16.
46. Kong DF. Aspirin in cardiovascular disorders. What is the optimum dose? Am J Cardiovasc Drugs. 2004; 4:151-8.
47. Wilterdink JL, Bendixen B, Adams HJ, Woolson RF, Clarke WR, Hansen MD. Effect of prior aspirin use on stroke severity in the trial of Org 10172 in acute stroke treatment (TOAST). Stroke. 2001; 32:2836-40.
48. Woolfe GJ, Melzig M, Schneider S, Dörr F. The Role of Tautomeric and Rotameric Species in the Photophysics of 2-(2'-hydroxyphenyl)benzoxazole. Chem Physics. 1983; 77:213-21.
49. Casey JR, Grinstein S, Orlowski J. Sensors and regulators of intracellular pH. Nat Rev Mol Cell Biol. 2010; 11:50-61.
50. Cai H. Hydrogen peroxide regulation of endothelial function: origins, mechanisms, and consequences. Cardiovasc Res. 2005; 68:26-36.
51. Zhu XY, Liu HC, Guo SY, et al. A Zebrafish Thrombosis Model for Assessing Antithrombotic Drugs. Zebtafish. 2016; 13:335-44.